A Neural Network Approach for Modelling Non Linear Transfer Functions: Application for Wind Retrieval from Spaceborne Scatterometer Data

by

S. THIRIA[*], C. MEJIA[*,**] , F. BADRAN[*] and M. CREPON[**]

[*] CEDRIC, Conservatoire National des Arts et Métiers
292 rue Saint Martin - 75003 PARIS

[**] Laboratoire d'Océanographie et de Climatologie (LODYC), T14, Université de PARIS 6
4 Place Jussieu - 75005 PARIS (FRANCE)

Abstract

The present paper shows that a wide class of complex transfer functions encountered in geophysics can be efficiently modelled by the use of neural networks. Neural networks can approximate numerical and non numerical transfer functions. They provide an optimum basis of non linear functions allowing a uniform approximation of any continuous function. Neural networks can also realize classification tasks. It is shown that the classifier mode is related to Bayes discriminant functions which give the minimum error risk classification. This mode is useful to extract information from an unknown process. The above properties are applied to the ERS1 simulated scatterometer data. When compared to other methods one finds that neural networks solutions are the most skillful.

Contents

1. INTRODUCTION

Transfer functions are widely employed in physics. They are mainly used to relate measured quantities to significant physical parameters under study. In many cases transfer functions cannot be determined from theoretical considerations and have to be estimated from a data set. As an example oceanographers and meteorologists expect to measure the sea surface wind by using spaceborne radar. Theory predicts some relationship between the backscatter signal of the radar and the wind vector but the complete problem is too complicated to solve. Experiments with airborne radars have been used to determine a semi empirical relationship for the backscatter signal as a function of the wind vector and of the incidence angle. But the determination of the wind vector from the radar signal leads to a very difficult inverse problem. In the present paper we propose a general method to determine such complex transfer functions empirically by using neural networks

Neural networks (henceforth NN) offer interesting possibilities for solving problems involving transfer functions [Rumelhart, 1986; Lippmann, 1987]. First, NN are adaptative providing a flexible and easy way of modelling a large variety of physical phenomena. Here, adaptive means the ability of the method to process a large number of data or to deal with new relevant variables Secondly, even if the learning (or calibration) phase of the network takes a long time, the operational phase is very efficient. This phase requires few calculations and can be carried out on small-sized computers. Moreover NN architecture is easily implemented on dedicated hardware using parallel algorithms, thus further reducing the processing time.

The aim of the present paper is first to show that NN are able to model a large class of complex transfer functions and secondly to give a theoretical framework for the use of NN in that context. In order to be as clear as possible we have chosen to deal with a particular example that demonstrates several different possibilities of NN.

In what follows, attention is focused on the retrieval of scatterometer winds by the use of Neural Networks. The method is presented in detail and can easily be extended to a large class of problems involving the computation of empirical transfer functions. The matter is of interest since the European satellite ERS1 with the AMI (Advanced Microwave Imager which can function in scatterometer mode) was launched in 1991 and the American scatterometer NSCAT (NASA SCATterometer) should be launched in 1996 on the Japanese satellite ADEOS. We have previously used NN to solve the scatterometer wind ambiguity removal problem [Badran *et al.*, 1991]. In the present work the scatterometer wind retrieval and ambiguity removal are integrated in a complete Neural Machine (NM) dedicated to computing horizontally consistent wind vectors from scatterometer backscatter measurements.

First an analysis of the physical problem is presented and its possible decomposition into different sub-problems is shown. The second section gives an overall presentation of NN and describes in detail how they have been used in this work. Some theoretical results are provided in order to offer a general method for approximating transfer functions; then some results using simulated data are presented. The third section presents the "Neural Machine" and displays the obtained results. Appendices give a deeper insight into the theoretical results.

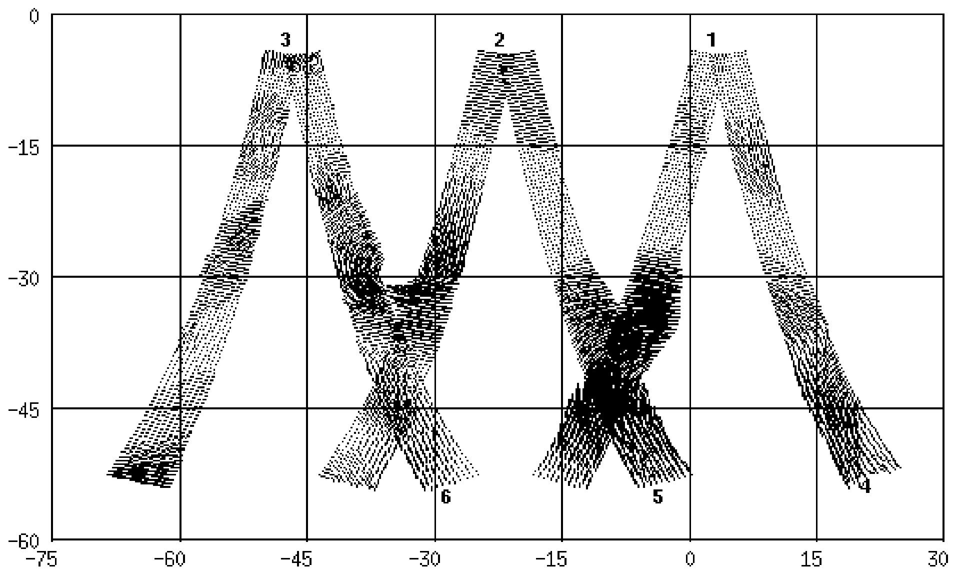

Figure 1 *: ERS1 satellite swath showing the upward and downward (ascending and descending) wind trajectories during three consecutive orbits.*

2. THE GEOPHYSICAL PROBLEM

2.1. BACKGROUND

The wind and the latent and sensible heat fluxes are the major forcing of the ocean circulation. As the spatial distribution of these parameters plays an essential role in driving the large scale circulation, a good knowledge of their space variability is of fundamental importance to understand and model ocean circulation.Scatterometers will provide measurements of the wind vector on a grid mesh of 50∞50 Km with a time and space coverage dramatically improved as compared to conventional means of observation. For the first time oceanographers can expect to obtain an adequate description of the forcing of ocean circulation which mainly depends on the wind-stress vector for the surface layers and on the wind-stress curl for the large scale and deep motions.

Scatterometers are active microwave radar which accurately measure the ratio of transmitted versus backscattered power signal, a ratio usually called the normalized radar cross section (σ^0) of the ocean surface.The physics of the interaction of the radar beam with a rough sea-surface is poorly understood. Such effects as wave breaking, modulation by long waves, and the effects of rain, make the problem complex.

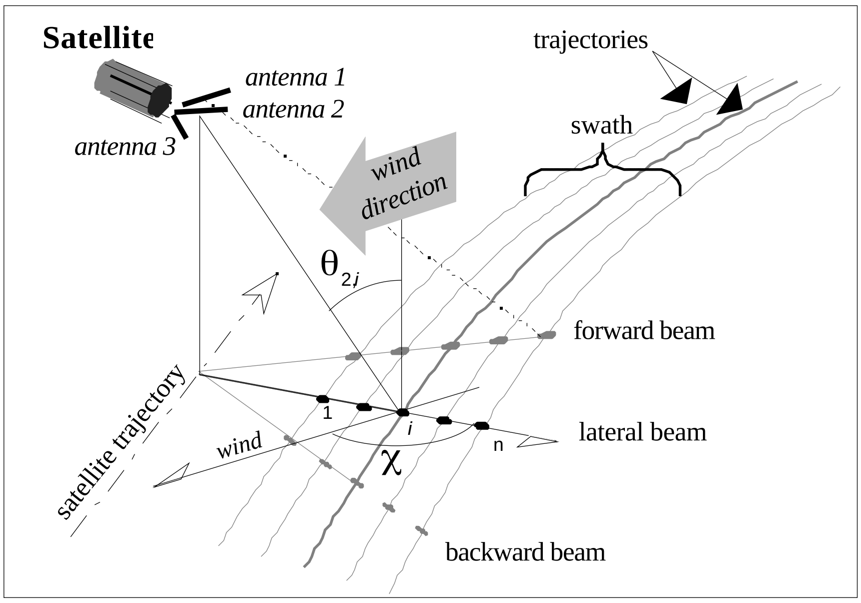

Figure 2 *: Definition of the geometry of the scatterometer observations.*

In fact empirical models have been proposed by geophysicists: they result from experimental research which has shown the strong dependence existing at the ocean surface between the σ^0 and the wind. An empirical relation can be determined by a functional equation of the form (Figure 2):

$$\sigma^0 = G(\chi,\theta,\varepsilon,v)$$

where σ^0 is expressed in dB and represents the ratio between the radar signal emitted and received .

G is a function of:

- The angle of incidence θ, measured on the vertical plane, between the incident radiation and the normal to the sea surface,
- The azimuth angle χ, measured on the horizontal plane, between the antenna and the wind direction,
- The radiation polarization ε, and

- The wind speed *v*.

Since it is found that the σ^0 varies harmonically with χ it is possible to compute the wind direction by using several antennas pointing in different orientations with respect to the satellite track (Price, 1976 - Freilich and Chelton, 1986).

A model developed by A. Long [Long, 1986] gives an expression for σ^0 which is approximated by a Fourier series of the form:

$$\sigma^0 = U \cdot \left(\frac{1 + b_1 \cdot \cos(\chi) + b_2 \cdot \cos(2\chi)}{1 + b_1 + b_2} \right)$$

with $U = A \cdot v^{\gamma}$

The parameters *A* and γ only depend on the incidence angle θ, b_1 and b_2 are a function of both the wind speed v and the incidence angle θ.The different parameters used in this model are determined experimentally.

The computation of the wind vector requires the inversion of the above formula

In the absence of noise introduced by the sensor or by the geophysical model, the three σ_0 given by the three antennas $(\sigma_1, \sigma_2, \sigma_3)$ at a given point enable the computation of the wind speed and the wind direction in a unique way, except at certain peculiar points where ambiguities exist (Figure 3a).

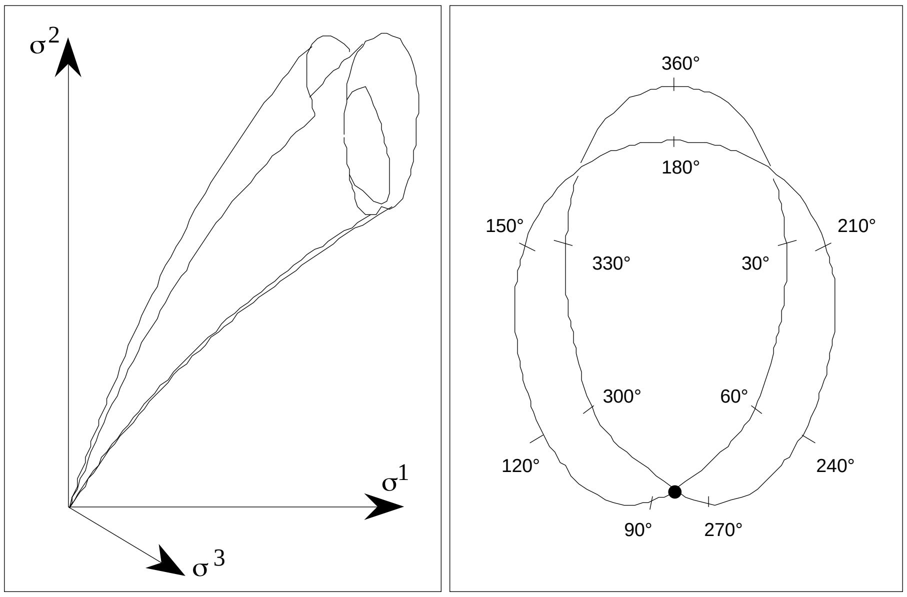

***Figure 3** : (a) Functional for computing the wind speed and direction as a function of the σ^0 measured by the antennas (b) Graph obtained for a section at constant wind speed.*

In the σ^0 space, the graph of the above function (Figure 3a) is a triple cone-like surface with singularities corresponding to ambiguities in the wind direction (Cavanié and Offiler, 1988 - Roquet and Ratier, 1988). The directrix is a Lissajous curve which is a function of the wind direction whereas a coordinate along the generatrix is a function of the wind speed. At a constant wind speed, the Lissajous curve implies that two directions differing by 150° are possible for some $(\sigma_1, \sigma_2, \sigma_3)$ measurements (Figure 3b).

The problem is therefore how to retrieve wind vectors using the observed measurements $(\sigma_1, \sigma_2, \sigma_3)$.

The determination of the wind vector may be decomposed into two different problems which are not of the same order of difficulty. Due to the Lissajous ambiguities, computing the wind speed is easier than computing the wind direction. Thus the whole problem can be decomposed into two sub-problems leading to the determination of two distinct transfer functions. The first one is a singlevalued function which permits the computation of the wind speed while the wind direction determination is a multivalued function. The aim of this preliminary study is to show that neural networks can efficiently solve such problems. The demonstration was made using simulated data and the results compared with of more traditional methods. We now present the data set used for the experimental part of the study.

2.2. THE SIMULATED DATA

As real data were not yet available, we have tested the method on simulated data computed from meteorological models. The swaths of the scatterometer ERS1 were created by simulating a satellite flying on wind fields provided by the ECMWF analysed output (Figure 1). The wind data were collocated to the simulated satellite measurements. The backscatter values $(\sigma_1, \sigma_2, \sigma_3)$ given by the three antennas were calculated using Long's model. Noise was then added to the σ_0 in order to simulate the errors made by the scatterometer and the small scale structures of the wind field (A gaussian noise of zero average and of standard deviation 9.5% for both lateral antennas and 8.7% for the central antenna was added at each measurement - see Appendix C). By way of comparison the actual instrument noise of the ERS1 scatt is about 5%. Thus our simulations take into account more than just instrument noise.

The data set used to calibrate the NN (the so-called learning set) was extracted from 22 maps (Figure 1) representing 22 days of satellite observation over the southern Atlantic ocean, regularly distributed over September 1986; the 9 days left were used to make the test. Results have been tested on a data set of 5041 wind vectors. These wind data are error free.

The statistics performed on the learning set showed that the winds have a velocity ranging from 4 to 20 m/s with an average of 8.24 m/s and a standard deviation of 3.03 m/s. As the directions become insignificant when the wind velocity is too weak, small amplitude winds (less than 3 m/s) were eliminated.

The learning sets must be choosen in relation to specific goals. Thus two different learning sets have been selected. The first one was selected in order to be statistically representative of the wind speed, and the second of the directions. This operation is fundamental to ensure the accuracy of the method. NN can be considered as statistical estimators and can only compute significant parameters when they are calibrated by using statistically significant learning sets. The first results obtained showed that some relation exists between the learning set's structure and the method's performances: in fact under-represented speed or direction could not be computed correctly.

In order to get realistic results when the network is operating and to check its generalization ability, the 9 maps used during the test were not used at all during the learning phase.

In the following it is shown that neural networks have theoretical properties which allow them to approximate complex transfer functions accurately. Section 3 is devoted to the approximation of transfer function through the use of neural networks. Section 4 presents the NM which solves the scatterometer remote sensing problem described above.

3. NEURAL NETWORKS

3.1. PRELIMINARIES

This section presents a basic discussion of Quasi-Linear Neural Network (QMN) which are the NN used in the present work; a more complete presentation is available in [Badran, 1991] and reviews on this technique are in [Rumelhart, 1986; Lippmann, 1987].

A **neuron** (or automaton) is an elementary transfer function which provides an output s (s [S)when an input A is applied.

$$s = f(A)$$

f is the transition function.

An **neural network** is a set of interconnected neurons (Fig. 5). Each neuron receives and sends signals only from the neurons to which it is connected (Fig. 4a). Thanks to this association of elementary tasks a neural network is able to solve very complicated problems. This ability is related to the number of neurons and to the topology of their connections.

In the following we assume that S = [-1, +1] . The state s_i of neuron i is a non-linear function f of the its **total input** A_i (Fig. 4b).

$$s_i = f(A_i) \qquad \text{with } A_i = \sum_h w_{ih} s_h \qquad (1)$$

where f is the sigmoid function with $f(u) = a \frac{e^{\alpha u} - 1}{e^{\alpha u} + 1}$ and h stands for the neurons connected to i. The w_{ih} are the **connection weights** from h to i.. They are real numbers weighting the various influences of the connected neurons. The matrix weight.**W** = $[w_{ih}]$ determines the specifity of the NN. The w_{ih} are computed by a calibration process, the so-called "learning process", where the input and output of the NN are well defined data sets and the w_{ih} the control variables.

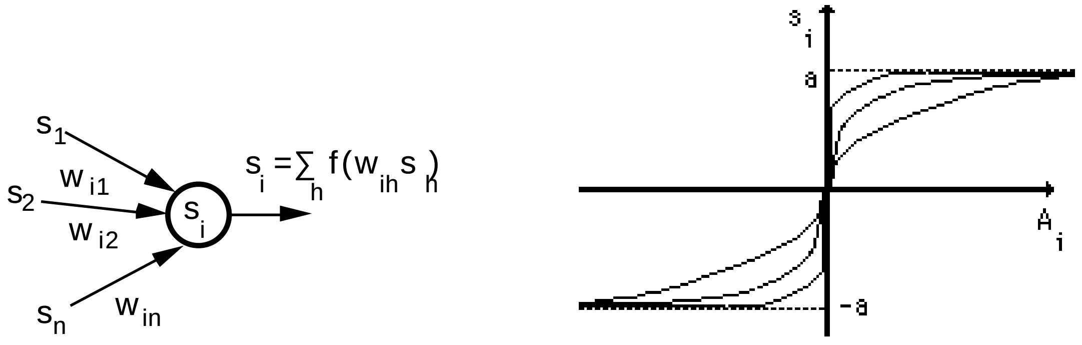

(a) *(b)*
Figure 4 : *(a) Diagram of a neuron (automata). (b) Sigmoid function f for different values of α . The figure shows different functions f for α varying from 4 to 1 (the greater α , the steeper the curve).*

In the present problem, we used Multi-layered Networks formed by several layers of neurons.

3.2. The Quasi-linear Multi-layered Networks (QMN)

Multi-layered architecture has one layer receiving the input, one layer which broadcasts output and one or more intermediate layers (the hidden layers) which are situated in between. All the networks we used are fully connected e.g. each automaton on a given layer is connected to all the neurons on the next one. The connection is one-way. The information progates from the input to the output. There are no connections within a particular layer. Such an architecture enables the association between sets of patterns or real numbers or more generally between m vectors ($\mathbf{x}_1,\ldots,\mathbf{x}_m$) (the input data), each $\mathbf{x}_k$ in $\leftarrow^{n}$, and m corresponding vector ($\mathbf{y}_1,\ldots,\mathbf{y}_m$) (the output data), each $\mathbf{y}_k$ in $\leftarrow^{p}$.

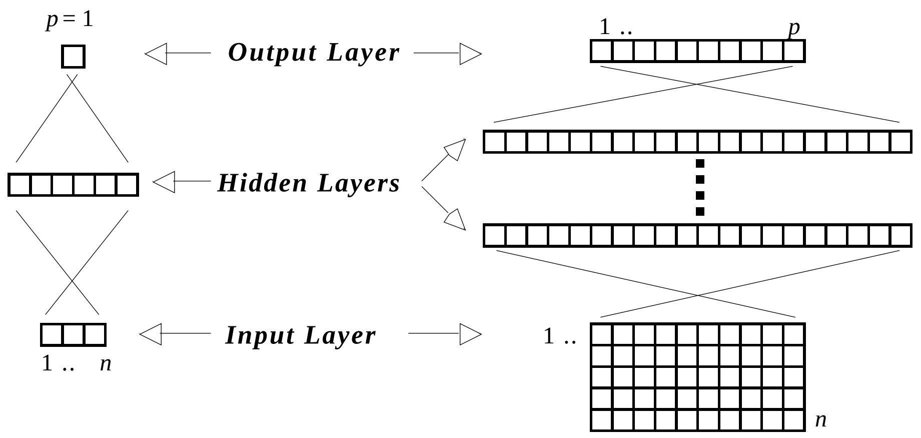

Figure 5: *two examples of simple architectures.*

First, the architecture is chosen (number of layers, number of neurons on each layer, the parameters a and α) on empirical considerations based on previous similar problems. The dimension n (number of neurons) of the input layer is chosen identical to that of the $\mathbf{x}_k$ vectors and the dimension of the output layer p identical to that of the $\mathbf{y}_k$. Then, during a learning phase, the network is trained to realize the desired associations ($\mathbf{x}_k$ $\mathbf{y}_k$, ($k = 1\ldots m$)); the w_{ih} are computed by using the back propagation algorithm described in the following.

The connection weights w_{ih} are initialized to random values. Then, an input $\mathbf{x}_k$ ($k = 1\ldots m$) is presented to the network; the states of the n neurons on the input layer are forced at the $\mathbf{x}_k$ values; these states are propagated through the different layers of the network by using rule (1). The state $\mathbf{s}_k$ of the last layer is called the computed output associated with $\mathbf{x}_k$. It is compared to the desired output $\mathbf{y}_k$ and an associated cost is defined as:

$$C_k = \|\, \mathbf{s}_k - \mathbf{y}_k \,\|^2 = \sum_{j=1}^{p} [s_{jk} - y_{jk}\,]^2$$

where j indexes the p neurons in the last layer.

The total cost is:

$$C(\mathbf{W}) = \sum_{k=1}^{m} C_k \tag{2}$$

The total cost C is then minimized using a stochastic gradient method. The successive modifications were performed using a second order stochastic gradient which is the approximation of the Levenberg-Marquardt rule [Battiti, 1992].

In order to be statistically significant the computation of the w_{ih} requires a learning data set whose number of elements m is ten times the number of w_{ih} .

At the end of the learning phase, the QMN is completely determined. Information or "knowledge" of the association is encoded into the connection weights w_{ih} and the QMN is able to generalize, e.g. to associate new sets of data which have not yet been learned. The learning phase may require long computations due to the minimization process. But during the operational phase the computation time is very fast because all the minimizations have been done during the learning phase and the only computations are algebraic operations. Indeed various real world applications have been implemented in speech recognition using neural networks which need, as in remote sensing, to deal with large amount of data [Lipmann, 1989]

3.3. TRANSFER FUNCTION APPROXIMATION USING QMN

A given architecture of QMN defines a family $\boldsymbol{F}$ of highly non-linear functions. Inside this family a particular QMN is characterized by its weight values.

The approximation of a multidimensional transfer function $\mathbf{T}(\mathbf{x})$ ($\leftarrow^{n} \quad \leftarrow^{p}$) with QMN can be done by using specific architectures (e.g particular families of function $\boldsymbol{F}$) whose first level has n cells and the last one p cells (Fig. 5). The number of layers and the number of cells on each layer is chosen in relation to the difficulty of the function $\mathbf{T}$ to be approximated (see APPENDIX A). Once the architecture is fixed, the best approximation of $\mathbf{T}$ (e.g the Least Mean Square approximation given in section 3.2) has to be found in the related family $\boldsymbol{F}$. The computed output values are expected to approximate $\mathbf{T}(\mathbf{x})$.

In Appendix A we discuss the theoretical results that if $\mathbf{T}$ is continuous on a compact subset, then $\mathbf{T}$ can be approximately represented by k-layer QMN ($k \geq 3$) in the sense of the uniform convergence [Blum, 1991; Cybenko, 1989; Funahashi, 1989; Hornik, 1989]. Moreover, the set of k-layer QMN provides a powerful set of basis of functions and theoretical results can often be experimentally extended to non-continuous mapping $\mathbf{T}(\mathbf{x})$. While the theory proves the existence of an architecture, it does not state how to choose it. Experimental results show that it is possible to derive a methodology to determine an adequate architecture.

3.4. HOW TO USE QMN CLASSIFIER PROPERTIES TO ANALYSE UNKNOWN NUMERICAL TRANSFER FUNCTIONS

One is often able to get measurements of a given phenomenon, but it is quite impossible to insert it in a conceptual framework. So it is of interest to extract some information embedded in the data: this could be the relevance of a given variable, information on the complexity of the phenomenon or the derivation of an analytical transfer function modelling it.

We have seen that QMN are able to approximate transfer functions. The simplest transfer functions we could imagine are numerical ones; a set of real vectors considered as input vectors are associated to another set considered as output vectors. QMN are well suited to model such functions even if they are non linear. QMN are also able to perform more complex even non numerical tasks.

In this section we present a methodology based on the latter QMN properties in order to get additional information on the complexity of the unknown transfer function. In fact the interpretation of the QMN outputs enables us to compute discrete values for **T**(**x**) with their related coefficients of likelihood [Bourlard, 1990]. This is necessary when studying complex multi-valued transfer functions which operate in a noisy environment. In that case, and for specific values of **x**, **T**(**x**) may have several possible values and thus it is inadequate to compute just one value for **T**(**x**). When dealing with scatterometer wind vector retieval the determination of the wind direction leads to such a problem. The problem is solved by determining the different possible values with their coefficients of likelihood.

In the following a method to compute the different values and their coefficients of likelihood is presented. The results obtained when using this method for the determination of the wind speed and the wind direction measured by satellite scatterometers are then discussed. More details about theoretical results and the generality of the approach are given in Appendix B and C [Gish, 1990; Geman, 1992, White 1989].

THE METHOD

Assume that **T** ranges on $[a, b]$; which is discretized in N intervals. The QMN is defined as before except for the output layer. This layer is made of N cells, each one stands for one interval; as an example cell i stands for the values of **T**(**x**) belonging to

$$I_i = \left[a + \frac{b-a}{N}(i-1), a + \frac{b-a}{N} i \right] \quad 1 \leq i \leq N$$

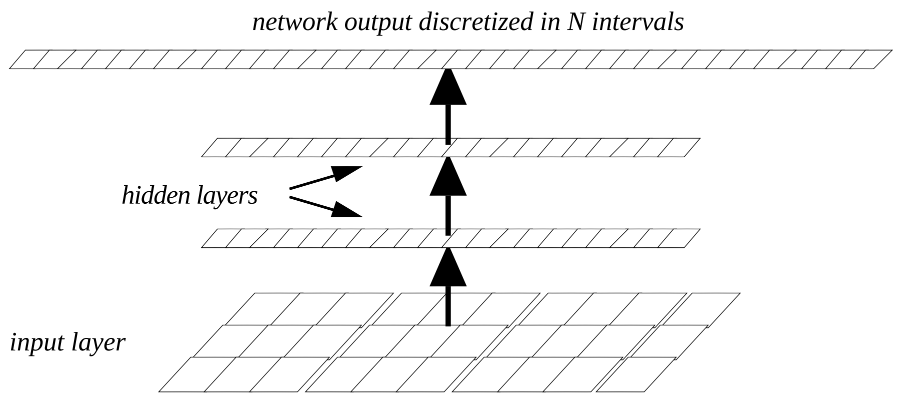

Figure 6 : *the figure represents a N output network for the discretizd approach*

An input pattern **x** is associated with class *i* if **T**(**x**) belongs to I_i. Approximating **T**(**x**) is now to learn the association {(**x**,*i*), **x** in $\leftarrow^n$}.

In order to associate a numerical value approximating **T**(**x**) we identify I_i by means of the centroid m_i

e.g $m_i = a + \frac{b-a}{N}\left(- \frac{1}{2}\right)$ stands for I_i

We now have to define the desired output. For a given input **x**, the desired output vector **y** = ($y_1, y_2, \ldots, y_N$) is coded by $y_i = +1$ if the value of **T**(**x**) is in interval I_i and $y_i = -1$ if not.

For a given weight matrix **W**, the QMN now approximates **T** using a function **F**(·,**W**) from ($\leftarrow^{n} \quad \leftarrow^{N}$) *N* being the number of intervals used to discretize **T**. The output associated to vector **x** is a vector **y** of dimensionality *N* defined by: (F_1(**x**,**W**), ..., F_N(**x**,**W**)). The process to determine the optimal mapping is the same as explained above:

Determination of the desired output **T**(**x**) = **y**

Computation of the network output **F**(**x**,**W**)

Minimization of the distance *C*(**W**) to get the Matrix **W** where

$$C(\mathbf{W}) = \sum_{k=1}^{m} \left\| \mathbf{F}(\mathbf{x}_k,\mathbf{W}) - \mathbf{y}_k \right\|^2 = \sum_{k=1}^{m} \sum_{i=1}^{N} \left(F_i(\mathbf{x}_k,\mathbf{W}) - \mathbf{y}_{ki} \right)^2$$

The QMN is now used as a classifier system. Theoretical results [Devijver, 1982; Duda, 1973; White, 1989] allow us to compare the optimal mapping **F**(**x**,**W***) computed by the back-propagation algorithm (**W*** are the optimum weights) and the Bayes classifier. It is found that **F**(**x**,**W***) gives the "best" approximation in $\boldsymbol{F}$ (family of functions associated to the QMN architecture) of Bayes discriminant functions. So the output values can be used as liklihood coefficients ; this allows us to rank the multiple solutions.(see APPENDIX B for exact relationships). Each cell *i* of the output layer, associates the value m_i with the related coefficient of likelihood $F_i(\mathbf{x},\mathbf{W}^*)$. Each input pattern **x** is thus associated to the output activation curve which is the graphical representation of the relation $(i, F_i(\mathbf{x},\mathbf{W}^*))$ (Fig.7). In this figure the *x*-axis represents the index of the output cells and the *y*- axis the output values $F_i(\mathbf{x},\mathbf{W}^*)$. A peak $(i, F_i(\mathbf{x},\mathbf{W}^*))$ of this curve is a local maximum which can be characterized by the cells $(i-1)$, i, $i+1$. The peak *i* is thus associated to a coefficient of likelihood $F_i(\mathbf{x},\mathbf{W}^*)$ and to a numerical value q_i which is the weighted average:

$$q_i = \frac{\sum_{j=i-1}^{i+1} F_j(\mathbf{x},\mathbf{W}^*) m_j}{\sum_{j=i-1}^{i+1} F_j(\mathbf{x},\mathbf{W}^*)} \qquad (3)$$

For each pattern **x**, owing to the number of significant peaks, the QMN gives L possible values of **T**(**x**) which are the q_{i_l} ($l = 1, .. L$). These values correspond to the L peaks having the best coefficient of likelihood. These peaks are ranked by decreasing order of their conditional probabilities $p(I_{i1} \mid \mathbf{x}) \geq \ldots \geq p(I_{iL} \mid \mathbf{x})$.

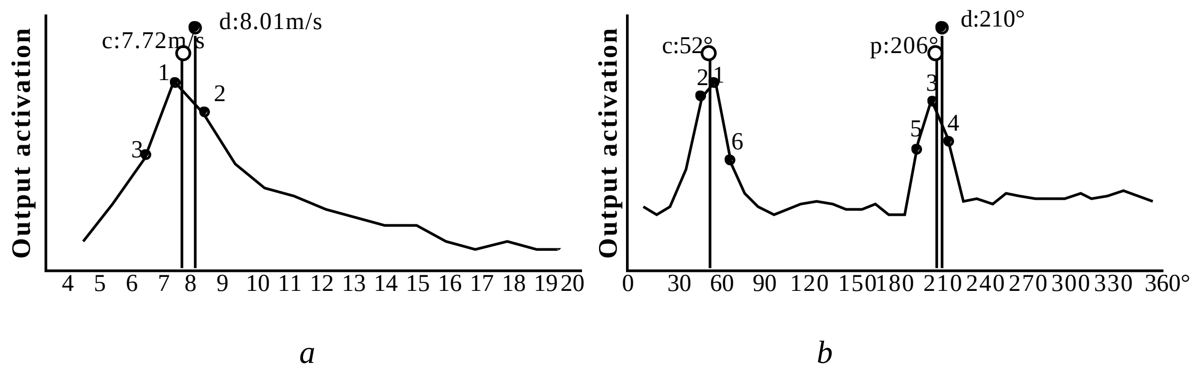

***Figure 7 :** Characteristic examples of output curves: (a) exhibits a single peak (which is a characteristic output for the speed); (b) exibits two major peaks (which is a characteristic output for the direction). The letter d represents the real solution on the x axis , c is the first significant peak computed by using formula 3, p the second peak*

The exact location of q_{i_l} on the *x*-axis permits the accurate computation of different possible values of **T**(**x**) and the corresponding *y*-axis gives the coefficient of likelihood. The values of the function are accurate because, although the values of **T**(**x**) have been discretized for the learning phase, the interpolation of the peaks curve allows $\mathbf{T}(\mathbf{x})$ to be continuous. Looking at the different curves obtained for each pattern of the learning set enables us to understand the “complexity” of the function studied. Figure 7 gives two characteristic examples of the output curves obtained with the approximation of the two transfer functions we deal with (determination of the wind speed (v) and of the wind direction (χ)) for a given input $\mathbf{x}$. The "complexity" of the phenomenon is related to the number of significant peaks. It clearly appears that the wind speed transfer function (Fig. 7a) is singlevalued and the related output curves exhibit a single peak. On the contrary the wind direction transfer function is multivalued (Fig. 7b), several peaks are present showing the existence of major ambiguities (two peaks or more).

In the following, the approach described here in which the output variable range is descretized, is called classifier mode, in opposition to the real mode in which the output variable is estimated directly without descretization.

3.5. NUMERICAL RESULTS

We now present results obtained using simulated scatterometer data. These results demonstrate the validity of the NN approach and its potential to give new insight into the geophysical function.

First it is noted that the geophysical function strongly depends on the incidence angle. In fact, the points located on the same parallel to the satellite trajectory are associated with a specific model (Fig. 3a); different parallels (hereafter called trajectories) lead to similar models which differ only in the values of the parameters (b_1, b_2, A, γ). Without any loss of generality we chose to study the central trajectory e.g. $(\theta_1,\theta_2,\theta_3) = (41.9°, 31.8°, 41.9°)$ and the two associated transfer functions $\mathbf{T_1}$ and $\mathbf{T_2}$. The transfer functions $\mathbf{T_1} : (\sigma_1, \sigma_2, \sigma_3)$ (v) and $\mathbf{T_2} : (\sigma_1, \sigma_2, \sigma_3)$ (χ) are approximated using both real and classifier QMN. Experiments were also made for others trajectories and similar results were found.

In the classifier mode as explained above the ranges of $\mathbf{T_1}$ and $\mathbf{T_2}$ have been discretized in the following manner : each interval I_i represents 1 m/s for the wind speed and 10°.for the wind direction For each experiment, statistically representative learning sets have been selected, which means that the QMN is trained with exactly the same number of patterns for each interval (this number will be indicated for each experiment later). Each example was randomly selected from the 22 maps used for the training (see § 2.2).

Determination of the wind speed

In the following we show how NN can be used to compute complex transfer functions and to extract information from unknown phenomena. Real and classifier QMN are used and then compared.

Geophysical measurements have shown that $\mathbf{T_1}$ is highly non-linear. This fact has been found from the results of preliminary experiments. The non linearity of $\mathbf{T_1}$ becomes important at the threshold value of 12 m/s. Therefore this information has been taken into account by splitting the interval into two sub intervals, each one being associated to a specific NN. Two sets of experiments were then performed to model the non-linearity of $\mathbf{T_1}$. The performances reached were compared. Moreover, for each experiment, dedicated neural networks were trained with both real and classifier QMN:

- the first approach consists in approximating the function on its total range [4m/s, 20m/s] by a single QMN.

- the second approach takes the nonlinearity into account ; the function $\mathbf{T_1}$ is then approximated with two different QMN. One is dedicated to low winds ranging from 4 m/s to 12 m/s, the other to high winds from 12 m/s to 20 m/s.

In order to take these differences into account and to make the performances of the two experiments comparable, the performances of the second experiment are given for each range separately and on the whole range (4 m/s-20 m/s). The performances are weighted by the frequency (number of data of a learning set over the total number of data) of each learning set (slow or high wind speed).

The architectures of the QMN used to run the experiments are now presented.

The inputs of the QMN are the $(\sigma_1, \sigma_2, \sigma_3)$ measured by the scatterometers. Owing to the space variability of the wind, the measurements at a given point are closely related to those occurring in the neighborhood (Fig. 8).

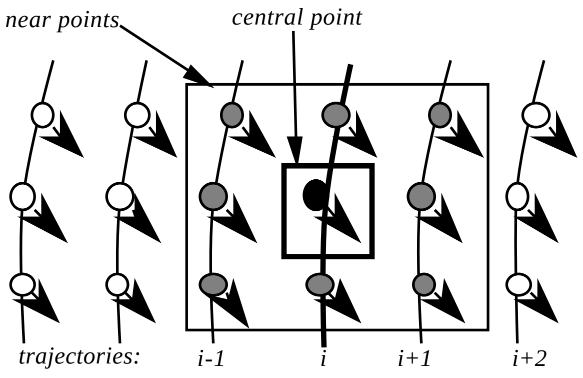

Figure 8 : *3∞3 space window related to the trajectory i .*

Taking this spatial context into account must therefore bring supplementary information to perform the task. Thus the input layer of each QMN consists of 27 neurons: these 9∞3 neurons correspond to the σ^0 values relative to the 3 antenna. The same experiments were performed without spatial context; they showed that the learning and test performances for speed were decreased by 17%, which proves the advantages of the spatial context. Each architecture is fully connected and has two layers of 25 units each; in the real mode a single output computes a single value for **T**(**x**), in the classifier mode there are 8 or 16 outputs (N = 8 or N =16), depending on the range considered (Fig. 9).

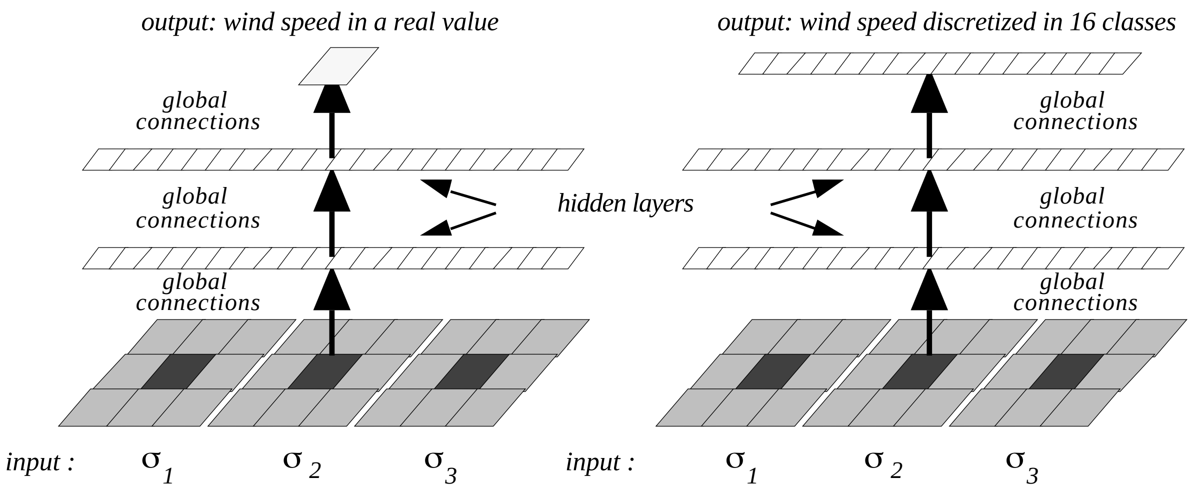
output: wind speed in a real value
output: wind speed discretized in 16 classes
global connections
global connections
global connections
hidden layers
global connections
global connections
global connections
input : σ_1 σ_2 σ_3
input : σ_1 σ_2 σ_3

Figure. 9 : *two different networks representing the wind speed respectively using the real (left) and the classifier (right) modes .*

Three data sets were built, allowing the training of the QMN within the following ranges (in m/s) [4, 12], [12, 20],[4, 20]; their sizes are respectively 6176 (772 for each interval of 1 m/s), 440 (55 for each interval), 6616 (6176+440). Therefore six QMN were trained. They were denoted by *[4,12]-QMN*, *[12,20]-QMN*, *[4,20]-QMN* adding "*-R*" or "*-C*" according to the mode. The performances of the six different QMN are now compared. The performances of the *[4,12]+[12,20]-QMN* are computed as explained above (as the sum of the two QMN dedicated to slow and high wind speed).

Tables 1 and 2 give the performances with the required accuracy; a computed output is considered as correct if it differs either by 1 m/s or 2 m/s from the desired value of the wind speed v . The performances of the learning phase represent the percentage of good approximation obtained from the learning sets, the test performances represent the percentage calculated on the 5041 examples of the test set (9 complete maps). The error, e is the mean of the absolute value of the error in estimating the wind speed made by the network . It is expressed in m/s

accuracy	wind speed	*[4,20]-QMN*	*[4,12]-QMN*	*[12,20]-QMN*	*[4,12]+ [12,20]-QMN*
± 1 m/s	**learning set**	98,0 %	99,3 %	98,9 %	99,3 %
	e	0,265 m/s	0,178 m/s	0,186 m/s	0,179 m/s
	test set	97,4 %	99,5 %	91,1 %	98.4 %
	e	0,294 m/s	0,189 m/s	0,421 m/s	0,220 m/s
± 2 m/s	**learning set**	100 %	100 %	100 %	100 %
	test set	99,8 %	100 %	99,7 %	100 %

Table 1 : *performances given by the three different QMN when approximating the wind speed transfer function using the real mode.*

accuracy	wind speed	*[4,20]-QMN-C*	*[4,12]-QMN-C*	*[12,20]-QMN-C*	*[4,12]+ [12,20]-QMN-C*
± 1 m/s	**learning set**	94,5 %	92.7%	98,6 %	93.1%
	e	0,342 m/s	0,435 m/s	0,134 m/s	0,405 m/s
	test set	91 3%	95.5%	90.7 %	94.9 %
	e	0,422 m/s	0,410 m/s	0,134 m/s	0,373 m/s
± 2 m/s	**learning set**	98.6 %	100%	98,6 %	99.9 %
	test set	97.3%	100 %	95,9 %	99.4 %

Table 2 : *performances reached by the three different QMN when approximating the wind speed transfer function using the classifier mode.*

For the two experiments (real and classifier mode) $\mathbf{T_1}$ is approximated with a good accuracy. The above results show a small decrease in performances and an larger error for the classifier mode. Nevertheless, when *[4,12]+[12,20]-QMN-C* is used, the loss is small. The weak results for *[12,20]-QMN-C* are due to the lack of data available for the training; this can be improved by using a larger number of data during the learning phase. However using the classifier mode gives a useful insight on function $\mathbf{T_1}$. The output curves exhibit a single significant peak as displayed in Fig.7a showing that $\mathbf{T_1}$ is single-valued.

Determination of the direction

Similar experiments were performed to determine $\mathbf{T_2}$. This function has been shown to be multi-valued. The accuracy of the results is now given in degrees; two values have been tested :

- ±20° which is the specification taken by oceanographers in order to compare the results with classical methods.

- ±10° in order to check the accuracy of the method.

At a given wind speed the wind direction is given by a Lissajous curve; this Lissajous curve is strongly dependent on the wind speed (Fig. 3). In order to be correctly positioned along the directrix of the curve presented in Fig. 3, the wind speed computed above is added onto the input layer as a supplementary information. This new information improves the accuracy of the solution. Thus the input layer of each QMN is now composed of 30 neurons: the first 9∞3 correspond to the σ_0 values for each antenna using the spatial window defined above, the last three correspond to the wind speed computed for the current trajectory in order to be correctly positioned along the directrix of the curve presented in Fig.3. The ratio of the weight given to the wind speed (3) versus the 9∞3 σ_0 values was chosen empirically and has not been optimized All the architectures are fully connected and have two layers of 25 units; in the real mode they have two outputs which compute the sine and cosine of the desired direction, and in the classifier mode 36 outputs (N = 36), each cell corresponding to an interval of 10° (Fig. 10).

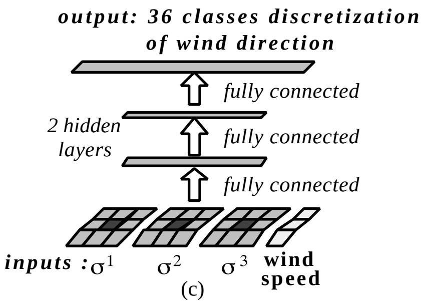

Figure 10 : *network representing the output direction using the classifier mode; the output range is discretized in 36 classes, each one representing 10°.*

Three learning sets were built so that wind directions were statistically homogeneous. Moreover, as for the wind speed approximation, several experiments were run according to the range of the wind speed: [4m/s, 12m/s], [12m/s, 20m/s] or [4m/s, 20m/s]; as explained above the learning sets have the same number of examples for each possible direction (interval of 10°). The size of the learning set is 5184 (144∞36) for [4m/s, 12m/s], 1098 (30∞36) for [12m/s, 20m/s], and 5904 (164∞36) for [4m/s, 20m/s].

The real approach was studied for the third range: [4m/s, 20m/s]. It gives one value of $\mathbf{T_2}(\mathbf{x})$ only. The classifier mode was studied by performing three experiments, one for each range. Four QMN were trained: *d-[4,20]-QMN-R*, *d-[4,12]-QMN-C*, *d-[12,20]-QMN-C*, *d-[4,20]-QMN-C* (the “ *d-*”

indicates that the direction is concerned). Performances were also computed on *d-[4,12]+[12,20]-QMN-C*.

The results are displayed in Tables 3 and 4, for both learning and test sets and for the two experiments. They are computed as they were for $\mathbf{T_1}$ but with a ±10° or ±20° accuracy. Several tests have been performed; for each test the performances are given so that the exact value of $\mathbf{T_2}(\mathbf{x})$ is among the first ***L***-peaks (***L*** = 1, 2, 3, 4) of the output curve provided by the networks. Table 4 shows that two peaks give a very good performance and four peaks help to fit function $\mathbf{T_2}$ quite perfectly.

accuracy	learning	test
±10°	52,9%	51,4%
±20°	75,6%	74,0%
±30°	84,9%	82,4%

Table 3 : *:performances (in %) on d-[4, 24]-QMN-R (**real mode**) with respect to three different accuracies.*

accu.	*d-[4,12]-QMN-C*	*d-[12,20]-QMN-C*	*d-[4,12]+[12,20]-QMN-C*	*d-[4,20]-QMN-C*	accu.	*d-[4,12]-QMN-C*	*d-[12,20]-QMN-C*	*d-[4,12]+[12,20]-QMN-C*	*d-[4,20]-QMN-C*
±10°-1p	62.7%	86.9%	66.9%	64.5%	**10°-1p**	69.3%	83.9%	71.3%	67.8%
±10°-2p	97.0%	99.7%	97.5%	93.5%	**10°-2p**	97.5%	96.1%	97.3%	91,9%
±20°-1p	63.9%	87.1%	68.0%	67.5%	**20°-1p**	70.6%	85.8%	72.6%	72,0%
±20°-2p	98.9%	99.9%	99.1%	98.3%	**20°-2p**	99.4%	98.2%	99.2%	98.4%
±20°-3p	100%	100%	100%	99.7%	**20°-3p**	99.9%	93.3%	99.8%	99.5%
±20°-4p	100%	100%	100%	99.9%	**20°-4p**	100%	100%	100%	99.9%

(a) *(b)*

Table 4 : *performances (in %) on the learning (a) and test sets (b) with two different accuracy ±10° and ±20° using the **classifier mode.** Each row displays the accuracy and the number of possible solutions allowed for $\boldsymbol{T_2}(x)$ (number of curve peaks).*

Figure 11 displays the errors made by the network *d-[4,20]QMN-C*; the distribution on the test set of the absolute value of the difference existing between the true $\mathbf{T_2}(\mathbf{x})$ and the most probable value for $\mathbf{T_2}(\mathbf{x})$ are shown. Dealing with an accuracy of ±20° on the test set, the figure shows that 72% of the wind directions are correctly retrieved by the first peak and the remaining errors are located at about ±180°. This value corresponds to the theoretical ambiguities of the Lissajous curve. Table 4 shows that with an accuracy of ±20° two peaks help to recover $\mathbf{T_2}(\mathbf{x})$ with a skill of 98%. In most cases the second peak corresponds to the intrinsic error of 180° displayed in Figure 11.

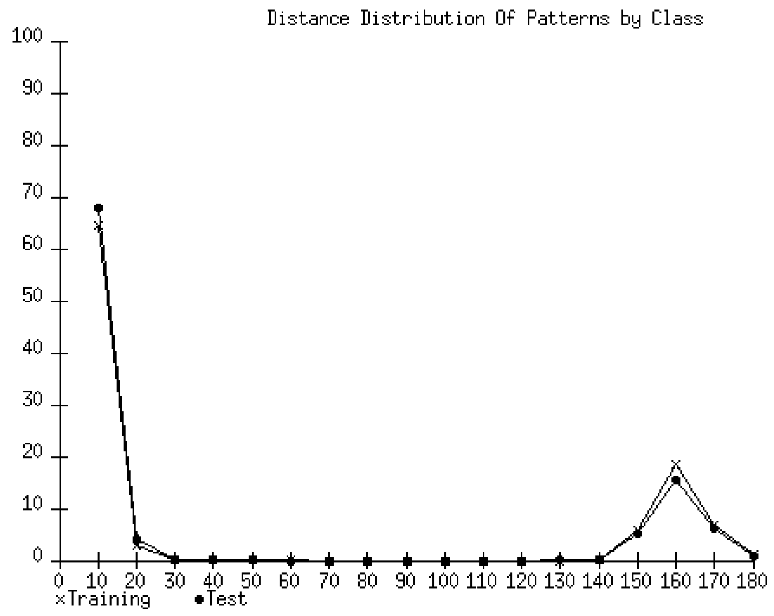

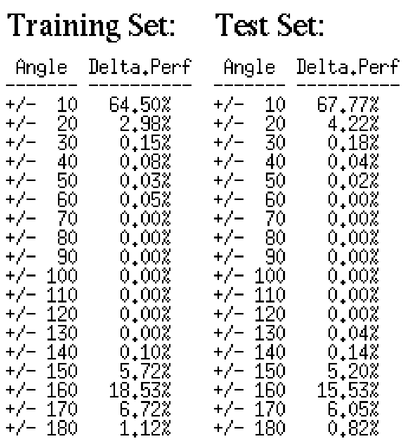

Training Set:		Test Set:	
Angle	Delta.Perf	Angle	Delta.Perf
+/- 10	64.50%	+/- 10	67.77%
+/- 20	2.98%	+/- 20	4.22%
+/- 30	0.15%	+/- 30	0.18%
+/- 40	0.08%	+/- 40	0.04%
+/- 50	0.03%	+/- 50	0.02%
+/- 60	0.05%	+/- 60	0.00%
+/- 70	0.00%	+/- 70	0.00%
+/- 80	0.00%	+/- 80	0.00%
+/- 90	0.00%	+/- 90	0.00%
+/- 100	0.00%	+/- 100	0.00%
+/- 110	0.00%	+/- 110	0.00%
+/- 120	0.00%	+/- 120	0.00%
+/- 130	0.00%	+/- 130	0.04%
+/- 140	0.10%	+/- 140	0.14%
+/- 150	5.72%	+/- 150	5.20%
+/- 160	18.53%	+/- 160	15.53%
+/- 170	6.72%	+/- 170	6.05%
+/- 180	1.12%	+/- 180	0.82%

Figure 11: *distribution of the absolute value of the difference between the true* $\boldsymbol{T_2(x)}$ *and the most probable value estimated by the d-[4,20]-QMN-C. Performances are given for both the training and the test set.*

Performances

In order to get an estimate of the performances of the NN method, the RMS wind vector error denoted e was computed by averaging over 10 000 independent wind estimations. All the simulations were processed on simulated data. The results are presented in table 5 . The above results show that the performances of NN are very good and of the same order at least as those described in Chi and Li (1988) for classical methods. These performances are linked to the ability of NN to model complex nonlinear phenomena without any statistical a priori information and their ability to take **spatial correlations** into account. The latter point deserves comments. In section 3.5 it has been shown that the use of spatial context improve the solution by a factor of 17%. Spatial correlations are easy to introduce when dealing with NN and more complicated when using conventional approaches. This can be considered as a major advantage of the NN method

Two to four wind solutions, the so-called "ambiguities", were usually obtained by using the wind estimation algorithm. The ambiguity that was the closest to the true wind vector was chosen as the estimated wind vector.

As mentioned in the introduction, the computation time of the method used to set up the wind map, which is an important aspect of the wind dealiasing algorithm, is very fast. The computation of a wind vector with NN requires approximately 12 ms on a SUN4 Spark Station.

Speed	*d-[4,20]-QMN-C*
low	0.32
Middle	0.40
Hight	1.18

Table 5 : *e (in m/s) for tthe [4,20]-QMN-C.*

The different QMN are now chained together in order to solve the complete problem which is the drawing up of a correct wind map. Section 4 presents the "Neural Machine". Section 4.1 is devoted to the presentation of the complete architecture. The results listed in section 4.2 deal with the same data as before.

4. THE "NEURAL MACHINE" (NM)

As we have seen, the wind speed and the wind direction are computed by two different modules composed of two and one QMN respectively. In fact the two modules are not independent. A Neural Machine [Thiria *et al.*, 1992] has accordingly been designed in order to connect them and to compute the wind vector automatically. The NM is formed by the association of three different modules. The first module $\mathbf{M}_1$ determines the wind speed at each point of the swath. The results are then supplied to the second module $\mathbf{M}_2$ as a supplementary data to compute the wind direction. A third module $\mathbf{M}_3$ removes the ambiguities on the direction. In order to take into account the strong dependence of the measurements with respect to the trajectory (e.g. the incidence angle, see Fig 12), each module consists of *n* (*n* being the number of trajectories in a swath) distinct but similar systems $\mathbf{S}_{ij}$ (i = 1,.,3 , j = 1,..,n) , a specific system being dedicated to each satellite trajectory (Fig. 13).

Within the same module $\mathbf{M}_i$, the different systems $\mathbf{S}_{ij}$ approximate similar transfer functions by using similar QMN. Consequently, the $\mathbf{S}_{ij}$ architectures for the same i are identical; the QMN associated to the $\mathbf{S}_{ij}$ only differ from each other by the numerical values assigned to the connection weights determined during the learning phase.

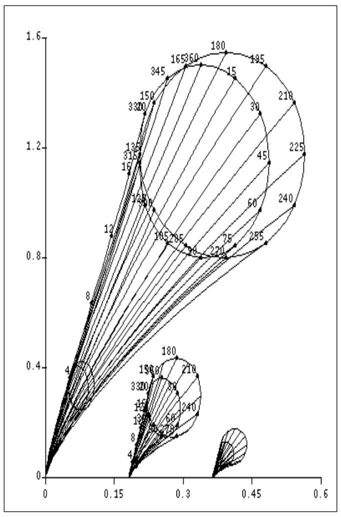

Figure 12 : *Projection of the geophysical model function onto the plane* $\sigma_1 \sigma_2$ *at three different incidence angles*

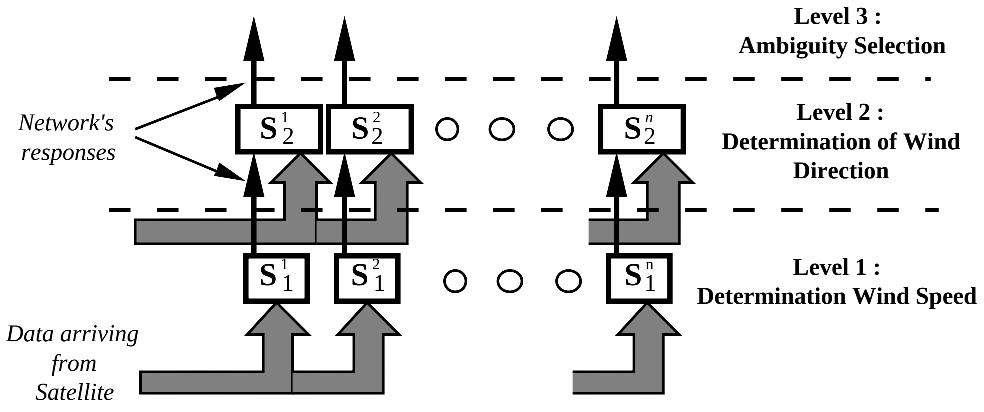

Figure 13 : *design of the Neural Machine (NM) . The NM is made of three different modules* $\mathbf{M}_i$*, each one being formed by n (number of trajectories in the swath) similar systems.*

In the first module $\mathbf{M}_1$ a system $\mathbf{S}_{1j}$ is devoted to the computation of the wind speed (in m/s) along the trajectory j (j = 1,.., n); the first module is made of n similar systems (one for each trajectory). Since the aim of the method is to compute the wind vector automatically from the measurements, each $\mathbf{S}_{1j}$ is made of three networks $\mathbf{R}_1, \mathbf{R}_2$ and $\mathbf{R}_3$ (see Fig. 14).

Given the procedure described in section 3.2 which takes into account the non linearities of $\mathbf{T_1}$, the system $\mathbf{S}_{1j}$ devoted to the numerical computation of the wind speed on the jth trajectory is approximated with two different networks $\mathbf{R}_2$ and $\mathbf{R}_3$ similar to the QMN described in section 3. They use the real mode and are respectively denoted*[4,12]-QMN-R* and *[12,20]-QMN-R*. .

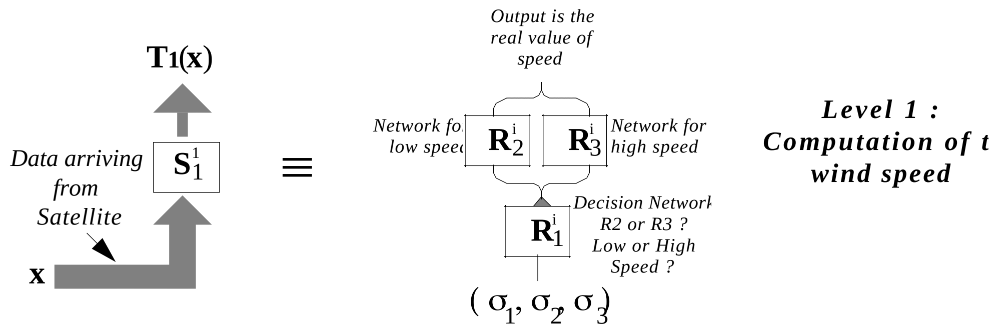
T1(x)
Data arriving from Satellite
x
S_1^1
≡
Output is the real value of speed
Network for low speed
R_2^i
R_3^i
Network for high speed
R_1^i
Decision Network R2 or R3 ? Low or High Speed ?
$(\sigma_1, \sigma_2, \sigma_3)$
Level 1 : Computation of t wind speed

Figure 14: *System $\boldsymbol{S}_{1i}$ used to compute wind speed.*

The first problem we have to face in computing v is to automatically select the correct QMN (either the *[4,12]-QMN-R* or the *[12,20]-QMN-R*.). This is done by using a switch network $\mathbf{R}_1$ which decides the range ($4 \le v < 12$ or $12 \le v < 20$) of *v*. The network $\mathbf{R}_1$ is a classifier which computes the probability of a slow or a high wind speed (*v*). It is a fully connected network whose inputs are the same as $\mathbf{R}_2$ and $\mathbf{R}_3$ (9∞3 neurons) ; it is composed of two hidden layers of 25 units and its output is made of two cells corresponding to the two ranges considered. For a given signal, the most active cell determines which QMN ($\mathbf{R}_2$ or $\mathbf{R}_3$) is activated for the computation.

In the second module a system ($\mathbf{S}_{2i}$) deals with a single network $\mathbf{R}_4$ which is the *[4,20]-QMN-C* of section 3 used in classifier mode.We recall that the input of $\mathbf{R}_4$ uses the wind speed as an additional information. The wind speed used here is computed by the first module of the NM (Fig. 15). Note that NM uses information embedded in the σ^0.

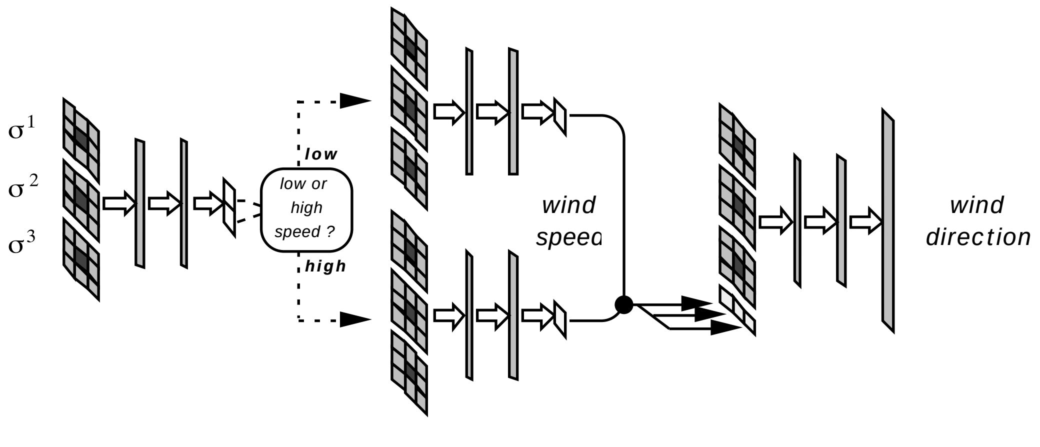

***R**$_1$* ***R**$_2$ and **R**$_3$* ***R**$_4$*

Figure 15 *Diagram of the NM. Architecture **R**$_1$ (classifier mode) for the input selection with respect to the wind speed, architectures **R**$_2$ and **R**$_3$ (real mode) for the wind speed computation, architecture **R**$_4$ (classifier mode) for the determination of the directions.*

As soon as the computation of the second module is achieved, the outputs provided by the two modules make the drawing of wind maps possible. As we have seen in the presentation of the physical problem, intrinsic errors due to the structure of the problem can remain. In most cases they appear as inverted directions at ±150°. These ambiguities have to be removed by a third module. The method has been described in [Badran *et al.*, 1991] and is not discussed here. It is related to image processing and deals with with a non linear space filter made of 5^5 neurons taking the context of the wind field into account . It enables us to correct up to 99.5% of the errors.

The whole process which merges the three modules together forms the NM which yields an automatic method for the computation of wind vectors.The NM is thus made of three modules, each one dedicated to the solution of one of the sub problems described previously. Within a same module the systems are similar and can work in parallel. The computation is performed sequentially between the different modules, each supplying the next with the parameters needed.

NUMERICAL RESULTS OF THE COMPLETE NEURAL MACHINE

We now present the results obtained for the central trajectory with the first two modules of the NM. The results computed with the two systems on the test set (9 maps, 5023 examples) are presented separately. In the simulations the two modules are linked, the $\mathbf{R}_1$ decision is strictly applied and the signal is processed by the most probable system $\mathbf{R}_2$ or $\mathbf{R}_3$. for computing the wind speed (v). This value is then used by $\mathbf{R}_4$ (the QMN of $\mathbf{S}_2$) to compute the wind direction (χ); the resulting wind vector is made of the two values $\mathbf{V'} = (v, \chi)$. So the results given by $\mathbf{S}_2$ include the error made in the determination of the wind speed by $\mathbf{S}_1$. We give the e_{rms} which now stands for the root mean square wind vector error $\mathbf{e}$; it is defined as follows: $\mathbf{e} = \mathbf{V} - \mathbf{V'}$ where $\mathbf{V}$ is the true wind vector and $\mathbf{V'}$ is the NM estimated wind vector, $e_{rms} = E(||\mathbf{e}||)$.When several solutions are considered together (p>1), the error $\mathbf{e}$ is equal to $\mathrm{Min}_{i=1,p}$ $\mathbf{V} - \mathbf{V}_i'$ where $\mathbf{V}_i'$ is the ith solution computed by $\mathbf{S}_2$.

$\mathbf{R}_1$ gives a correct switch in 97% of the cases, all the errors occurring around the threshold value of 12 m/s, between 10 and 14 m/s. Table 6 gives the performances for the wind speed ($\mathbf{R}_2$ corresponds to the low wind speed NN and $\mathbf{R}_3$ to high wind speed) and the related e_{rms} in m/s. Table 7 gives the performances for the wind direction and the e_{rms} for the output of the NM machine with two accuracies (10° and 20°).The performances correspond to the probability for one computed peak (p=1) or one among several (p=n) to be the right solution. In the latter case it is necessary to remove the ambiguities according to the method presented in Badran et al (1991)

accuracy	R_2 perf	R_2 e_{rms}	R_3 perf	R_3 e_{rms}
± 1m/s	98,9%	0,202 m/s	89,9%	0,432 m/s
± 2m/s	99,7%	0,202 m/s	99,0%	0,432 m/s

Table 6 : *wind speed computation : performances reached by the first module on the test set.*

accuracy	perf	e_{rms}
±10°-1p	61,2%	5,24 m/s
±10°-2p	84,2%	1,73 m/s
±20°-1p	69,5%	5,24 m/s
±20°-2p	95,8%	1,28 m/s
±20°-3p	97,6%	1,07 m/s
±20°-4p	99,0%	0,90 m/s

Table 7 : *wind direction computation : performances reached by the Neural Machine on the test set with two different accuracies of ±10° and ±20°; "ip" indicate that i peaks of the output curves have been used in order to compute* $\boldsymbol{T_2(x)}$.

Tables 6 and 7 show that the NM is able to automatically compute the wind vector from the scatterometer measurements alone. The use of two peaks gives good performances and 4 peaks help to recover the desired vector almost perfectly.

This study is a theoretical work, which has to be considered as a feasibility phase. Indeed actual values for the σ^0 were not available at the beginning of this study, all experiments were carried out on scatterometer simulated data obtained by applying Long's formula to winds computed by meteorological models. This formula is considered as a good representation of the actual phenomenon, and all wind estimation algorithms use similar formula. As mentioned above (see the comparison with other methods) all these algorithms use an analytical expression of σ^0 to compute the wind vector. On the contrary, Neural Networks compute an approximation of the desired transfer function without any a priori analytical and statistical hypothesis. This approximation is computed during the learning phase from significant examples and **one could show that it is the best approximation with respect to a large class of non linear functions modeled by QMN**. Because Long's formula was learnt with success, one may hope that thanks to this technique many similar problems will be solved. Theoretical results and the present study insure that any continuous and singlevalued transfer function can be adequately modelled by a NN which can be considered as a numerical interpolator.

In case of multivalued transfer functions we propose to use the classifier mode. The output of the NN are related to Bayes discriminant functions which give the *a posteriori* probability for the class *i* to be a solution. This enables us to get the different solutions and to rank them. Theoretical calculations show that assuming some regularity of the transfer function (an hypothesis often met in physics) the above Bayes discriminant functions are easy to approximate with NN. In appendix C it is shown that the Bayes discriminant functions approximated by the NN can be expressed from the geophysical model function which is of interest (the geophysical model function is often much more simple than the transfer function itself). So it is expected that the present study can be extended to a large class of problems dealing with transfer function of the same complexity ; NN architecture as small those used in this paper would provide similar results.

CONCLUSION

The aim of the present paper was to show that Neural Networks (NN) can model a large class of complex transfer functions. Moreover it provides a theoretical framework for the use of NN. In the sake of clarity we have chosen to deal with a particular example which highlights the different possibilities of NN. Attention has been focused on the decoding of satellite scatterometer data. The transfer function from the radar measurements (σ_o) to the wind vector is a very complex multivalued function. The wind speed is a non linear function with respect to σ_o and several solutions can be obtained for the wind direction. The complexity of the transfer function is shown in Fig. 2. It has been found by dealing with satellite simulated data that Neural Networks can solve this problem efficiently, accurately and quickly.

Several aspects of NN have been investigated. From a numerical point of view it has been shown that NN are suitable to approximate highly non linear functions. This is confirmed by the accuracy obtained on the computation of the wind speed. A theoretical proof of the validity of the method is given in appendix A. NN solution is the best approximation with respect to an optimum basis of non linear functions which are not fixed a-priori as in the classical least square fitting.

Emphasis has then been placed on the classifier properties of NN. In appendix B it is shown that the classifier mode of NN is related to Bayes discriminant functions which find the minimum error risk classification. This formalism allows us to realize switches or to solve multivalued functions. The solution of the problem under study is discretized in N intervals. The output layer is made of N cells, such that the cell i is linked to the interval I_i of the discretized solution. It can be shown that the state of a cell i is related to the *a posteriori* probability for the value of the studied transfert function to belong to the interval I_i when an input $\mathbf{x}$ is presented. Such a NN can be interpreted as a classifier. Using such a process enables to find several possible solutions to multivalued problems and to rank them.

In the scatterometer problem a complete Neural Machine has been proposed in order to obtain unambiguous wind vectors. Several aspects of the classifier mode have been used in the determination of the wind vector measured by scatterometers. In order to better fit the non linear aspect of the transfer function, the wind speed is computed by two different NN, one being devoted to low speed winds, the other to high speed winds. A classifier NN is used as a switch to sort high wind speed versus low wind speed and turn the input towards the dedicated NN. This switch improves the accuracy of the computation by allowing the computations to be done by an adequate NN. The wind direction is also determined by a NN used in classifier mode. In many cases several directions corresponding to several significant coefficients of likelihood are found. The remaining ambiguities are then removed by assuming that there is some space coherence of the wind vector [Badran et al, 1991] .

In section 3 several methods to retrieve the scatterometer wind have been compared. It appears that the NN have the best performance. From the above complex example we can claim that NN constitute a powerful tool to model a large class of transfer functions. In fact the NN are able to solve many problems encountered in physics. A major advantage of NN is their ability to extract information in a noisy environnement whatever the noise.

It has been found that NN are suitable to model non linear filters. Filtering is a technique often used in geophysics to remove noise or to take advantages of the information embedded in time intervals or space contexts. Such a filter has been used with success to remove the scatterometer wind ambiguities by Schlutz (1990). NN provides the optimum filter with respect to the studied problem (Badran *et al* , 1991).

NN are also suitable to solve complex inverse problems. The direct problem provides a suitable basis of examples which can be learned the other way around , the output of the direct problem being considered as the input of the inverse problem. The NN then computes a statistical model of the inverse problem. In fact the simulated scatterometer example presented in this paper can be considered as an inversion of Long's formula.

NN present many other advantages. It is very easy to take into account new parameters even if their dependence cannot be established in the form of an equation. New cells related to these new parameters are added to the input layer and connected to the hidden layers. In the scatterometer case it would be easy to investigate how sensitive the solution is to the introduction of additional variables such as wind waves which are supposed to influence the transfer function at low wind speed.

The methodology developed in the present study will be applied to ERS1 scatterometer data as soon as they are available. The determination and calibration of a Geophysical Model can be bypassed. In fact the Geophysical Model is embedded in the architecture of the NN machine described above. The NN machine will be calibrated during a learning phase on the output provided y a fine grid mesh meteorological model such as the PERIDOT model of the French Met Office (Météo-France). It is during this confrontation with the real world that the usefulness of NN should be definitely established.

Acknowledgments

This work was supported by CNRS (Centre National de la Recherche Scientifique), PNTS (Programme national de Télédétection Spatiale) and SGDN (Service General de la Défense Nationale). The simulations were run by using the SN2 software provided by the Neuristic Compagny. We are grateful to V. Cassé and C. Gaffard for stimulating discussions. We thank P. Braconnot and M. Boukthir for providing the data set. Useful comments were provided by an anonymous referee.

APPENDICES

APPENDIX A

QMN AND FUNCTION APPROXIMATION

The main theorem leads to the approximation of continuous mappings by QMN with k layers of hidden units e.g we call them k-layer QMN, where k stands for the number of hidden layers. The following result may be demonstrated [Cybenko, 1989; Funahashi, 1989; Hornik, 1989]:

Let **K** be a compact subset of $\leftarrow^n$ and let **T** : **K** $\quad \leftarrow^p$ be a continuous mapping defined by :

$$\mathbf{x} = (x_1, x_2, \ldots, x_n) \qquad (T_1(\mathbf{x}), \ldots, T_p(\mathbf{x}))$$

Then for any $\varepsilon > 0$; one can find a 1-layer QMN whose output layer neurons are linear (the transition function f is the identity) such that:

$$max_{\mathbf{x} \quad \mathbf{K}} \|\mathbf{T}(\mathbf{x}) - \mathbf{F}(\mathbf{x},\mathbf{W})\| < \varepsilon$$

where $\mathbf{F}(\cdot,\mathbf{W})$ is the function approximated by the 1-layer QMN

The above result only proves the existence of such a 1-layer QMN, ε -approximating the continuous mapping **T** on the compact subset **K** of $\leftarrow^n$. However this result does not indicate how to built the network, that is how to choose the number of hidden units: this has to be done heuristically with respect to similar problems studied previously. Further experimental results have shown that adding more hidden layers enables one to reach a given ε -approximation with fewer hidden units and connections [Lipmann, 1987].

Recent results [Blum, 1991] give upper bounds for the number of hidden units when using 2-layer QMN of a particular class, the class in which the transition function of the hidden units is the threshold function :

$$f(x) = 1 \text{ if } x \geq 0 \text{ and } f(x) = 0 \text{ if } x < 0$$

(f is thus a limit case of the classical sigmoid function) and when the output units linear. For every continuous mapping **T** on a compact subset **K**, **T** is uniformly continuous, then the following proposition holds:

$$\varepsilon > 0, \ \exists\ \omega(\varepsilon) \textit{ such that } \|\mathbf{x} - \mathbf{y}\| < \omega(\varepsilon) \textit{ gives } \|\mathbf{T}(\mathbf{x}) - \mathbf{T}(\mathbf{y})\| < \varepsilon$$

where $\omega(\varepsilon)$ is defined as the modulus of continuity.

It is shown that the ε -approximation can be done with $m\infty(4\infty n + 1)$ connections, $2\infty m\infty n$ units on the first hidden layer and m units on the second, with m the smallest integer greater than $\frac{1}{\omega(\varepsilon)}$. The determining factor $\omega(\varepsilon)$ which directly depends on **T** allows to understand the necessary complexity of the needed network.

We use networks with sigmoïdal transisition function in this application, these networks behave like almost peacewise-constant functions. So the preceeding result can be used to estimate an order of complexity for the studied problem. The larger ω the smoother the function. In the following this propriety will be used to show that the studied functions are smooth enough to be learned with small architectures.

APPENDIX B

CLASSIFIER MODE AND BAYES DISCRIMINANT FUNCTIONS

QMN has been widely used as classifiers. The classical approach is to use Bayes discriminant functions. The Bayes discriminant functions guarantee the minimum error risk of classification. These two approaches are closely related as described here .

The Bayes theory assumes an a-priori knowledge of the probability distribution of the data. Usually the density function is chosen in a given family. In order to give some theoretical insight on the way QMN and Bayes classifier behave we consider a N classes classification problem. The following notations are used :

$C_1, C_2, \ldots, C_N$: are the classes to be learned

X is the learning set.

x is an element of **X**.

$P(\mathbf{x})$ the density function of **x**.

$p(C_i \mid x)$ the probability of the class C_i given x.

A Bayes decision rule is defined by :

$$decide\ C_i\ if\ p(C_i \mid \mathbf{x}) = sup_j\ (p(C_j \mid \mathbf{x}))\quad j \quad [1 \ldots N]$$

Considering the function $g = (g_1, g_2, \ldots, g_N)$ called a Bayes discriminant function where

g_i (x) = $p(C_i \mid \mathbf{x}) - \sum_{i \neq j} p(C_i \mid \mathbf{x})$; the above rule can be rewritten

$$\textit{decide } C_i \textit{ if } \; g_i(x) = sup_j \left(g_j(x)\right) \quad j \in [1 \ldots N]$$

let us now focus on the QMN approach. In order to built the QMN classifier one have to defined the desired outputs of the network, that is the coding of the different classes. In most cases the desired outputs are the index of the classes : for a given pattern $\mathbf{x}$ of class C_i, the desired output is thus $\mathbf{y} = (y_1, \ldots, y_N)$ with $y_i = +1$ for C_i and $y_j = -1$ else.

It can be shown [Gish, 1990; White, 1989] that, given a particular architecture $\mathbf{F}(\cdot,\mathbf{W}) = (f_1, f_2, \ldots, f_N)$ and a large learning set $\mathbf{X}$:

$$C(\mathbf{W}) = \sum_{\mathbf{x} \quad \mathbf{X}} \left\|\mathbf{F}(\mathbf{x},\mathbf{W}) - \mathbf{y}\right\|^2 \approx \sum_k \int \left[f_k(\mathbf{x}) - g_k(\mathbf{x}) \right]^2 P(\mathbf{x})\, d\mathbf{x} + Constant$$

Thus the back-propagation algorithm which minimizes $C(\mathbf{W})$ gives a function

$\mathbf{F}(\cdot,\mathbf{W}) = (f_1, f_2, \ldots, f_N)$ which approximate the Bayes discriminant functions $(g_1, g_2, \ldots, g_N)$. The approximation is in the sense of the probability weighted least sqares of the above formula.

The states of the output units $f_k(\mathbf{x})$ are thus linked to the *a posteriori* probability $P(C_k \mid \mathbf{x})$. It is straightforward to show that $f_k(\mathbf{x})$ can also be interpreted as coefficients of likelihood. The accuracy of the approximation depends on the complexity of the *a posteriori* probability function (annex A), the architecture of the QMN and on the learning set $\mathbf{X}$ [Geman, 1992; Vapnik, 1982; White, 1989].

APPENDIX C

Accuracy of the approximation for the classifier mode

Let us now discuss the accuracy of the approximated function computed using the QMN classifier mode. The demonstration is given for the wind direction transfer function. Similar results can be given for similar problems.

Notations are as follow:

v : is the wind speed,

χ : is the azimuth angle,

$\hat{\sigma}$: $(\hat{\sigma}_1(\chi,v),\hat{\sigma}_2(\chi,v),\hat{\sigma}_3(\chi,v))$ is a parametrical representation of the geophysical model function defined in the σ_O space (see Figure 2a) and

I_i : $i = 1, \ldots, 36$ are the 36 classes of 10° each: I_i stands for: $10\,(i-1) \le \chi < 10\,i$.

Let us assume that the learning set has been determined using an uniform distribution for the wind speed and the wind direction and that the noise added to the model are normally distributed:

- The (χ,v) have been sampled at random using the uniform distribution on $\leftarrow = [0,360]\quad[4,20]$, thus the density function of (χ,v) is

$$: q(\chi,v) = \frac{1}{360\quad 16}\, 1_{\leftarrow}, \qquad (3)$$

$1_{\leftarrow}$ is the characteristic function of rectangle $\leftarrow$.

- $\hat{\sigma}(\chi,v)$: $(\hat{\sigma}_1(\chi,v),\hat{\sigma}_2(\chi,v),\hat{\sigma}_3(\chi,v))$ is computed using the Long formula (§2.1).

The simulated measurements σ : $(\sigma_1,\sigma_2,\sigma_3)$ is generated by adding a gaussian noise to the computed $\hat{\sigma}(\chi,v)$, i.e. $\sigma_i - \hat{\sigma}_i(\chi,v)|_{i\,=\,1,\,2,\,3}$ are normally distributed with zero mean and standard deviation s. Thus the density function of the measurements can be written:

$$p(\sigma \mid \chi,v) = \frac{1}{(s\sqrt{2\pi})^3} \cdot e^{-\frac{\left\| \sigma - \hat{\sigma}(\chi,v) \right\|^2}{2s^2}} \qquad (4)$$

Using (4) $p(\sigma,v)$ and $p(I_i,\sigma,v)$ can be computed:

$$p(\chi,v,\sigma) = p(\sigma \mid \chi,v)\, q(\chi,v) \qquad (5)$$

$$p(\sigma,v) = \int_0^{360} p(\chi,v,\sigma)\, d\chi \quad \text{and} \quad p(I_i,\sigma,v) = \int_{10(i-1)}^{10\,i} p(\chi,\sigma,v)\, d\chi \qquad (6)$$

and finally an explicit expression for the *a posteriori* probability of interest is given : $p(I_i \mid \sigma,v) = \dfrac{p(I_i,\sigma,v)}{p(\sigma,v)}$

The Bayes decision function can then be computed:

$$g_i(\sigma,v) = \frac{p(I_i,\sigma,v)}{p(\sigma,v)} - \sum_{j \ne i} \frac{p(I_j,\sigma,v)}{p(\sigma,v)} \quad \text{for } i = 1,.\,, 36 \qquad (7)$$

S =

Erreur!

Equations (3), (4), (5), (6) prove that the Bayes discriminant functions $g_i(\sigma,v)$ for the wind direction approximation are smooth functions as long as the actual function $\hat{\sigma}(\chi,v)$ is smooth itself. So, the modulus of continuity $\omega(\varepsilon)$ (see annex A) is large enough to allows a good approximation using small QMN with few hidden units. Such a remark explains the results provided by the experiments: a good approximation has been reached by a small 2-layers QMN with 2 hidden layers of 25 hidden units each.

Moreover this demonstration is quite general in the sense that similar conclusions can be deduced for the determination of the wind direction. This can be done also for any physical phenomenon assuming that the transfer function to look for is smooth enough, which is often the case when dealing with actual phenomena in physics.

The above formulas show that the Bayes decision functions take into account the statistical distribution of the wind, the error of the measuring devices and the transfer function at the same time ; this enables us to use the numerical analysis properties and the statistical ones simultaneously.

REFERENCES

Badran, F., S. Thiria, and M. Crepon, Wind ambiguity removal by the use of neural network techniques, *Journal of.Geophysical.Research*, 96, NO. C11, 20 521-20 529, Nov 15, 1991.

Battititi, R., First and second order Methods for learning: Between Steepest descent and Newton's Method, *Neural computation*, *4*, 141-166, 1992.

Blum, E., and L. Li, Approximation theory and feedforward networks, *Neural Networks*, *4*, 511-515, 1991.

Bourlard, H., and C.J. Wellekens, Links between Markov models and multilayer perceptrons, *IEEE Transaction. Pattern Anal. Machine Intell*, *12*, 1167-1178, 1990.

Cavanié A. and D. Offiler : ERS1 Wind Scatterometer : Wind Extraction and Ambiguity Removal. *Proceedings of IGARS 86 Symposium, Zurich*, (ESA SP-254), 1986

Cybenko, G., Approximation by superposition of sigmoidal function, *Mathematics of Control, Signal and Systems*, *2*, 303-314, 1989.

Devijver P., and J Kittler, Statistical Pattern Recognition, *Prentice Hall*, 1982.

Duda, R. O., and P.E Hart, Pattern Classification and Scene Analysis, *John Wiley*, New York, 1973.

Freilich, M.H., and D. B. Chelton, Wave number spectra of Pacific winds measured by the Seasat scatterometer, *J. Phys. Oceanogr.*, 16, 741-757, 1986.

Funahashi, K.I., On the approximate realization of continuous mappings by neural networs, *Neural Networks*, *2*, 183-192, 1989.

Geman, S., E. Bienenstock, and R. Doursat, Neural Network and the Bias variance dilemna, *Neural computation*, *4*, 1-58, 1992.

Gish, H., A probabilistic approach of the understanding and training of neural network classifiers, *ICASSP*, *3*, 1361-1364, New Mexico, 1990.

Hornik, K., M. Stinchcomb, and H. White, Multi-layer feedforward networks are universal approximators, *Neural Networks*, *2*, 359-366, 1989.

Lecun, Y., Boser B, Henderson D.,Howard R.E.,Hubbard and Jackel L.D. : Handwritten digit recognition with a back-propagation network, *Neural information Processing Systems* 2, 396-404, ed by D.S. Touretzki, Morgan Kaufmann.

Lipmann, R.P., An introduction to computing with neural nets, *IEEE ASSP Magazine*, 4-21, 1987.

Lipmann, R.P., Rewiew of neural netwoks for speech recognition, *Neural Computation, 1*, 1-38, 1989.

Long A. E. Towards a C-Band Radar Sea Echo Model for the ERS1 Scatterometer. *Proc. First Int. Coll. on Spectral Signatures, ESA, Les Arcs*, 1986

Price J. C. The nature of Multiple Solution of Surface Wind Speed Over the Oceans from Scatterometer Measurement. *Remote Sensing of Environement, 5*, 47-74, American Elsevier Publishing Compagny, 1976

Roquet, H. , and Ratier A., Toward direct assimilation of scatterometer backscatter measurements into numerical weather predction models, Proceedings of the *IGARSS'88 Symposium, Eur. Space Agency Spec. Publ. ESA* SP-284, 257-260, 1988

Rumelhart, D.E., J.L. MacClelland, and the PDP Research Group, *Parallel Distributed Processing: explorations in the microstructures of cognition*, MIT Press, 1986

Schultz, H., A circular median filter approach for resolving directionnal ambiguities in wind fieldd retrieved from spaceborn scatterometer data, *J. Geophys. Res.*, 95, 5291-5304, 1990.

Thiria, S., C. Mejia, F. Badran, and M. Crepon, Multimodular Architecture for Remote Sensing Operations, *Neural Information Processing System, 4*, R. Lippmann, J.E. Moody, Touretzky Ed., 1992.

Vapnik, V., *Estimation of dependences based on empirical data*, Springer Verlag, New York, 1982.

White, H., Learning in Artificial Neural Networks: A Statistical Perspective, *Neural Computation, 1*, 425-464, 1989.

Widrow, B., S.D. Stearns, *Adaptative Signal Processing*, Prentice Hall, Englewood Cliffs NJ, 1985.